International Journal of Automotive Technology, Vol. 7, No. 7, pp. 803–812 (2006)

1229–9138/2006/031–06

INTEGRATED VEHICLE CHASSIS CONTROL WITH A MAIN/SERVO-LOOP STRUCTURE

D. LI[1)*], X. SHEN[1)] and F. YU[1,2)]

[1)]200240 RM 327 Automotive Building, Institute of Automotive Engineering, Shanghai Jiao Tong University, No. 800 Dongchuan Road, Shanghai, China

[2)]State Key Laboratory of Vibration, Shock and Noise, No. 800 Dongchuan Road, Shanghai, China

(Received 18 April 2006; Revised 19 July 2006)

ABSTRACT–In order to reduce the negative effects of dynamic coupling among vehicle subsystems and improve the handling performance of vehicle under severe driving conditions, a vehicle chassis control integration approach based on a main-loop and servo-loop structure is proposed. In the main-loop, in order to achieve satisfactory longitudinal, lateral and yaw response, a sliding mode controller is used to calculate the desired longitudinal, lateral forces and yaw moment of the vehicle; and in the servo-loop, a nonlinear optimizing method is adopted to compute the optimal control inputs, i.e. wheel control torques and active steering angles, and thus distributes the forces and moment to four tire/road contact patches. Simulation results indicate that significant improvement in vehicle handling and stability can be expected from the proposed chassis control integration.

KEY WORDS : Vehicle dynamics, Chassis control integration, Longitudinal slip ratio control, Four wheel steering, Direct yaw moment control, Tire nonlinearities

NOMENCLATURE

a : distance from front axle to vehicle CG
a_{x_d} : desired longitudinal acceleration by driver
b : distance from rear axle to vehicle CG
c_1, c_2, c_3: tire modeling parameters
d_f, d_r : front and rear wheel track widths
F_L : tire longitudinal force in traveling direction
F_{uL} : tire forces along vehicle longitudinal axis
F_S : tire lateral force perpendicular to traveling direction
F_{uS} : tire forces perpendicular to vehicle longitudinal axis
F_u : vehicle motion forces and yaw moment vector
F_{WL} : tire longitudinal force in the wheel plane
F_x, F_y : vehicle longitudinal and lateral forces
g : constant of gravity acceleration
I_{zz} : vehicle moment of inertia of yaw
K : nominal understeer characteristic
L : vehicle wheelbase
M_z : vehicle yaw moment
m_v : mass of entire vehicle
r_{eff} : wheel efficient rotational radius
s_{Res} : resultant tire slip ratio
s_L, s_S : tire longitudinal and lateral slip ratios
u, v, r: vehicle longitudinal ,lateral and yaw velocities
v_R, v_W : wheel rotational velocity and wheelvelocity
α_f, α_r : front and rear tire slip angles
μ_{Res} : tire adhesion coefficient
μ_L, μ_S : longitudinal and lateral components of adhesion coefficient
f, r : front/ rear
i=1–4 : front left, front right, rear left and rear right

Abbreviation
4WS : four wheel steering
ABS : anti-lock braking system
DOF : degree of freedom
DYC : direct yaw moment control
LSC : longitudinal slip ratio control
TCS : traction control system

*Corresponding author. e-mail: duffayli@gmail.com

1. INTRODUCTION

Over the past twenty years, various mechatronic systems for vehicle chassis control, e.g. ABS/TCS, 4WS and active suspension, have been developed and brought into the market, resulting in significant improvement in vehicle handling and ride comfort. However, due to the essential dynamic coupling among vehicle subsystems, separately-developed control strategies could not overcome the increasing complexity and unfavorable interactions of subsystems, which in return demands more and more

sophisticated consideration of both software and hardware aspects (Fruechte *et al.*, 1989). Therefore, individual functions of the subsystems, e.g. steering, braking, and traction, must be dependently and cooperatively controlled to achieve the best overall performance of vehicle, which is the so-called integrated vehicle chassis control.

Among those pioneer works, an integrated control system of active suspension, front wheel steering and ABS/TCS was designed for real vehicle models (Yokoya *et al.*, 1990; Kawakami *et al.*, 1992), and its advantages were evidently presented. Based on LQR optimal control theory, the coordination between suspension and steering was investigated (Harada and Harada, 1999). Moreover, different cooperative control approaches for suspension and braking system were proposed and evaluated (Smakman, 2000; Nouillant *et al.*, 2002; Valasek *et al.*, 2004).

But more frequently, the integration of longitudinal and lateral dynamics, e.g. direct yaw moment control (DYC) and active steering, has been investigated extensively based on different control strategies (Horiuchi *et al.*, 1999; Manning *et al.*, 2000; Shino *et al.*, 2002; Cherouat *et al.*, 2004; Mokhiamar and Abe, 2004; Kim *et al.*, 2006). This is because active steering and DYC are basically two preferable chassis control systems to improve vehicle handling and stability. Furthermore, since its primary principle is to achieve a stabilizing yaw moment from differential longitudinal forces between left and right tires, DYC could not utilize tire lateral forces directly and thus it is less effective in lateral motion control. On the other hand, active steering has a significant effect on lateral control by adjusting tire slip angles and thus providing demanded lateral forces. But due to tire nonlinearities, its effectiveness is considerably reduced when tire/road contact is near saturation region (Furukawa and Abe, 1997). With this in mind, the integration of active steering and DYC can certainly provide a promising improvement in both lateral and yaw motion control.

However, most literatures on integrated vehicle control are focused only on the main loop design, i.e. the desired stabilizing lateral force and yaw moment are supposed always available under any situations. Less consideration was taken in actual tire force generation and distribution mechanisms. But due to tire nonlinearities and underlying vehicle dynamic coupling, this kind of main-loop design is sometimes too optimistic and can not provide sufficient accuracy and effect of stability control. Therefore, it is necessary to further consider tire nonlinearities and also how the stabilizing forces and moment can be optimally distributed to each tire. Hattori *et al.* (2002) proposed a nonlinear force distribution method, and the optimum distribution is achieved only through longitudinal slip ratio regulation. Emphasizing on tire workload, Mokhiamar and Abe (2004) proposed an optimal distribution method based on a weighted cost function which only includes tire workload. Shen *et al.* (2006) also proposed a chassis control integration based on μ-synthesis approach in the main-loop, and it also considered the actual forces and moment distribution.

Based on the foregoing studies, this research investigates a main/servo-loop based control integration between longitudinal slip ratio control (LSC) and active steering control, taking into account both actual tire force generation and optimum force distribution. More specifically, in order to ultimately divide the entire vehicle stability control problem into the control task and actual control actuation, the four nonlinear tires in the servo-loop are treated as special *actuators* to generate the desired stabilizing forces and moment for the whole vehicle, i.e. the *plant* in the main-loop, just as a general *controller-actuator-plant* control problem. As a result, the force optimal distribution can be solved as a force tracking problem through sequential quadratic programming approach, based on a weighted cost function including both force tracking error and control input limit consideration.

This paper is organized as follows: Section 2 addresses a nonlinear tire model and vehicle dynamics; Section 3 states the proposed chassis control integration in details, including the main-loop and servo-loop design; Section 4 presents the numerical simulations and the proposed integration design is also compared with the individually equipped LSC and 4WS cases; finally, Section 5 gives the conclusions of the research.

2. VEHICLE MODELING

2.1. Nonlinear Tire Model

A simple Burckhardt approach (Kiencke and Nielsen, 2000) is used to describe the tire combined slip characteristics. The modeling details are summarized in Equations (1)–(5) as follows.

$$\mu_{Res}(s_{Res}) = c_1 \cdot (1 - e^{-c_2 \cdot s_{Res}}) - c_3 \cdot s_{Res} \tag{1}$$

$$s_{Res} = \sqrt{s_L^2 + s_S^2} \tag{2}$$

$$s_L = \begin{cases} (v_R cos\alpha - v_w)/v_w, & v_R cos\alpha \le v_w \\ (v_R cos\alpha - v_w)/(v_R cos\alpha), & v_R cos\alpha > v_w \end{cases} \tag{3}$$

$$s_S = \begin{cases} (1 + s_L)\tan\alpha, & v_R cos\alpha \le v_w \\ \tan\alpha, & v_R cos\alpha > v_w \end{cases} \tag{4}$$

The resultant tire longitudinal and lateral forces F_L and F_S are defined in the direction of wheel traveling velocity v_w and the direction perpendicular to it, as can be seen in Figure 1. The force calculation can be carried out as

$$\begin{cases} F_L = \mu_L F_Z = s_L \cdot F_Z \cdot \mu_{Res}/s_{Res} \\ F_S = \mu_S F_Z = s_S \cdot F_Z \cdot \mu_{Res}/s_{Res} \end{cases}, \tag{5}$$

in which the equivalent wheel rotational velocity v_R is estimated as the product of wheel angular velocity $\dot{u}$ and effective wheel radius r_{eff}.

In above equations, tire slip angle α can be computed as $\alpha_f = \delta_f - \sigma_f$ and $\alpha_r = \delta_r - \sigma_r$, where angles σ_f and σ_r of front/rear axles can be estimated as $\sigma_f = \text{atan}[(v+ar)/u)]$ and $\sigma_r = \text{atan}[(v-br)/u)]$, respectively.

By using the above equations, the tire longitudinal force F_L and lateral force F_S changing with varying slip ratios and slip angles are plotted in Figure 2.

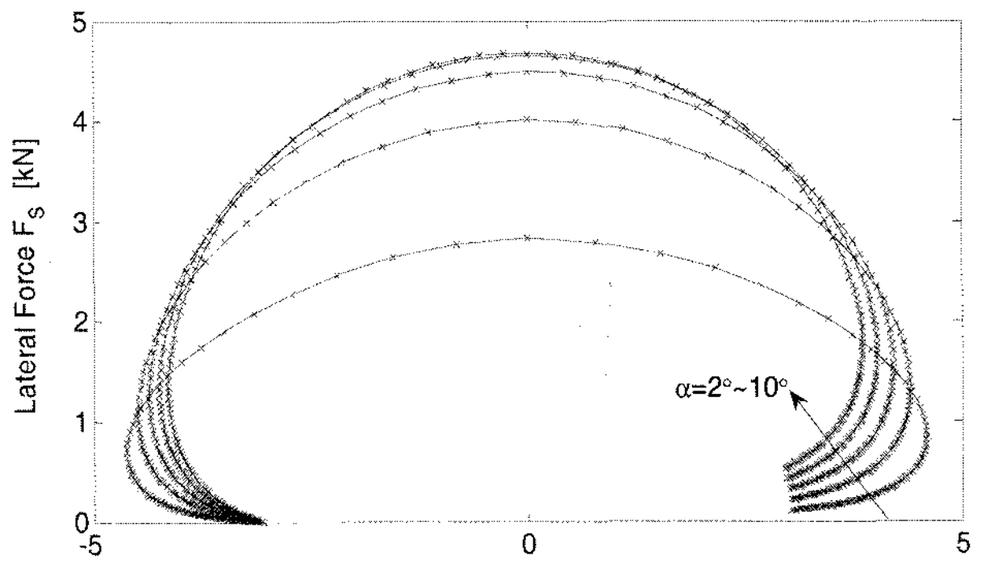

Figure 2. Characteristics of tire force with combined slip. (dry asphalt, $F_Z = 4$ kN, $s_L = 1$–1, $\alpha = 2°$–$10°$)

2.2. Total Forces and Moments on Vehicle Body

The forces of each tire should be further transformed into the vehicle coordinate system x_u-y_u for vehicle motion force calculation, as indicated in Figure 3.

Referring to Figure 1, the contribution that the front left tire makes to the total forces and moment can be calculated as

$$\begin{cases} F_{x1} = F_{L1} \cdot cos(\sigma_f) - F_{S1} \cdot sin(\sigma_f) \\ F_{y1} = F_{L1} \cdot sin(\sigma_f) + F_{S1} \cdot cos(\sigma_f) \\ M_{z1} = F_{L1} \cdot (asin\sigma_f - d_f cos\sigma_f/2) \\ \quad + F_{S1} \cdot (acos\sigma_f + d_f sin\sigma_f/2) \end{cases} \tag{6}$$

Therefore, the total forces $\boldsymbol{F}_u$ developed from four tires can be summarized as follows

$$\boldsymbol{F}_u = [\boldsymbol{F}_x \ \ \boldsymbol{F}_y \ \ \boldsymbol{M}_z]^T = M_F \cdot F_t, \tag{7}$$

where the tire forces are $\boldsymbol{F}_t = [F_{L1\sim4} \ \ F_{S1\sim4}]^T$, and the directional matrix $\boldsymbol{M}_F$ is

$$M_F = \begin{bmatrix} a_1 & a_1 & a_2 & a_2 & -b_1 & -b_1 & -b_2 & -b_2 \\ b_1 & b_1 & b_2 & b_2 & a_1 & a_1 & a_2 & a_2 \\ l_1 & l_2 & l_3 & l_4 & l_5 & l_6 & l_7 & l_8 \end{bmatrix} \tag{8}$$

The elements of $\boldsymbol{M}_F$ can be expressed as:

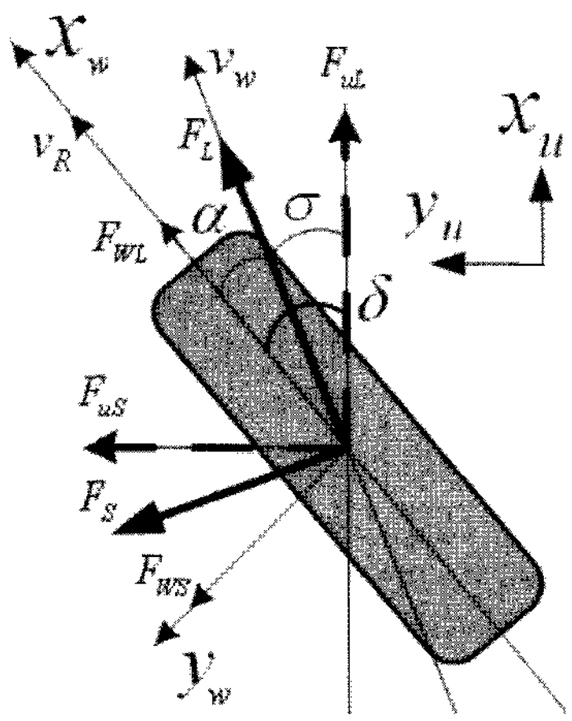

Figure 1. Forces of front left tire.

$$a_1 = cos\sigma_f,\ a_2 = cos\sigma_r,\ \ b_1 = sin\sigma_f,\ b_2 = sin\sigma_r,$$
$$l_1 = -a_1 d_f/2 + b_1 \cdot a,\ l_2 = -a_1 d_f/2 + b_1 \cdot a,$$
$$l_3 = -a_2 d_r/2 - b_2 \cdot b,\ l_4 = -a_2 d_r/2 - b_2 \cdot b,$$
$$l_5 = b_1 d_f/2 + a_1 \cdot a,\ l_6 = -b_1 d_f/2 + a_1 \cdot a,$$
$$l_7 = b_2 d_r/2 - a_2 \cdot b,\ l_8 = -b_2 d_r/2 - a_2 \cdot b.$$

3. INTEGRATED VEHICLE CHASSIS CONTROLLER DESIGN

As mentioned before, the control integration is implemented into the main and servo loop as diagrammatized in Figure 4. In this section, the reference vehicle model is given first, and then the details of main-loop and servo-loop controller design are presented.

3.1. Reference Model

As is well known, for vehicle stability control, vehicle sideslip angle should be suppressed as small as possible,

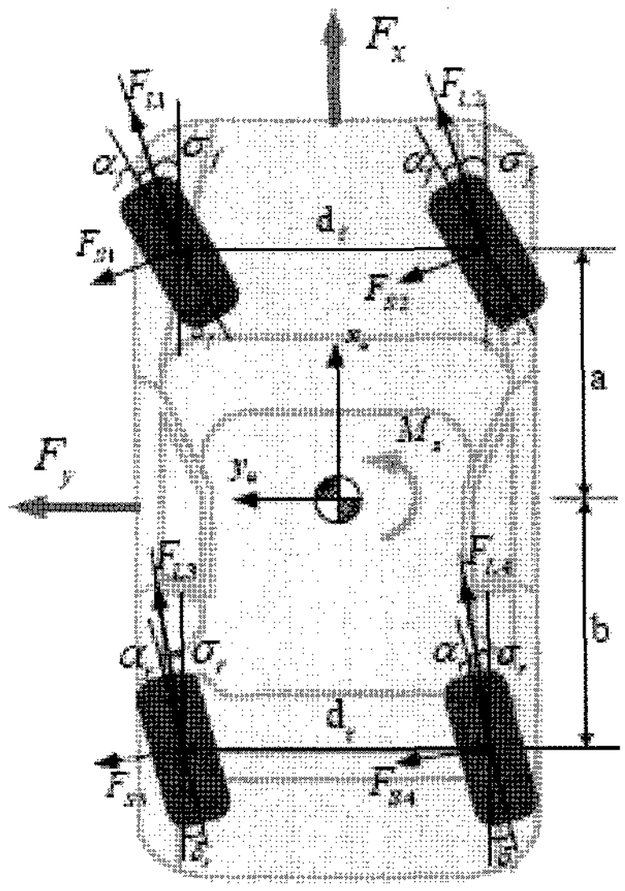

Figure 3. Vehicle model.

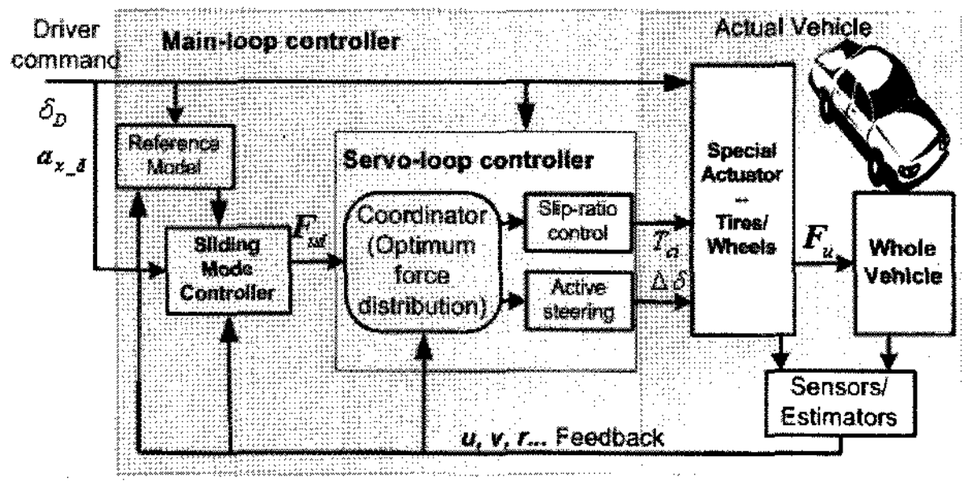

Figure 4. Scheme of the control integration based on main-loop and servo-loop structure.

so the desired lateral velocity is

$$v_d = 0 \tag{9}$$

The desired yaw rate r_d can be derived from the designed understeer characteristics, i.e.

$$r_d = \frac{1}{1+Ku^2}\frac{u}{L}\delta_D, \tag{10}$$

where K is the desired understeer gradient, and u is the longitudinal velocity.

To avoid large lateral acceleration that exceeds tire cornering capability (Kiencke and Nielsen, 2000), the yaw rate is constrained as

$$|r_d| \le |\mu_{Res}| \cdot g/u. \tag{11}$$

Additionally, as for acceleration or deceleration maneuver, the commanded longitudinal acceleration can be detected from foot pedal position. Therefore, neglecting the delay effect of driver response, the desired vehicle longitudinal velocity can be written as follows

$$u_d = u_0 + \int_0^t a_{x\_d}(\tau)d\tau. \tag{12}$$

3.2. Main-loop Control Design

According to the feedforward and feedback information, particularly, the tracking errors between the desired and actual values of longitudinal, lateral and yaw velocities, the main-loop controller computes the desired total forces and moment, i.e. F_{xd}, F_{yd} and M_{zd}, which are to be optimally distributed in the servo-loop to four tire/road contact patches.

Since the tire is treated as a special actuator as shown in Figure 4, the tire nonlinearities are then moved to the servo-loop. Therefore, the control task can be made easier, and a simplified model with 3 DOFs, i.e. longitudinal, lateral and yaw motions of vehicle body, can be adopted for the main-loop control design purpose, as shown in Equation (13).

$$\begin{cases} \dot{u} = vr + U_1/m_v \\ \dot{v} = -ur + U_2/m_v. \\ \dot{r} = U_3/I_{zz} \end{cases} \tag{13}$$

where the control inputs are

$$U = [U_1 \ U_2 \ U_3]^T = [F_{xd} \ F_{yd} \ M_{zd}]^T.$$

For robustness consideration, a sliding mode controller is employed. The nonlinear control problem in the main-loop can be rewritten as

$$\dot{X}_i = f_i(X,t) + g_i(X,t)\cdot U_i \tag{14}$$

where the system states are $X = [u \ v \ r]^T$..

Due to measurement noise and other model uncertainties, the dynamic parts $f_i(X,t)$ and $g_i(X,t)$ might deviate from their nominal values, but the deviations can be bounded as $|\Delta f_i| = |f_i - \hat{f}_i| \le F_i$ and $0 \le \beta_i^{-1} \le g_i \hat{g}_i^{-1} \le \beta_i$, where $\hat{f}_i$ and $\hat{g}_i$ are the nominal values of f_i and g_i, $F_i > 0$ and $\beta_i = (g_{imax}/g_{imin})^{1/2}$..

In order to suppress the tracking error $e_i = X_i - X_{id}$, and to reduce the steady state error, a composite sliding surface, namely proportional-integral sliding surface, is used (Slotine and Li, 1991),

$$S_i = e_i + \lambda_i \xi_i, \tag{15}$$

where $\lambda_i > 0$, and $\xi_i = \int_0^t e_i(\tau)d\tau$.

The derivative of sliding function in Equation (15), is

$$\dot{S}_i = \dot{e}_i + \lambda_i e_i = f_i + g_i \cdot U_i - \dot{X}_{id} + \lambda_i e_i \tag{16}$$

Defining $\hat{u}_i = -\hat{f}_i + \dot{X}_{id} - \lambda_i e_i$, the control law that satisfies the sliding condition can be obtained as

$$U_i = \hat{g}_i^{-1}[\hat{u}_i - k_{1i}S_i - k_{2i}sgn(S_i)]. \tag{17}$$

with $k_{1i} > 0, \eta_i > 0$, and

$$k_{2i} \ge \beta_i(F_i + \eta_i) + (\beta_i - 1)|\hat{u}_i| \tag{18}$$

In fact, by substituting Eqation (17) into Equation (16), there exists

$$\begin{aligned} \dot{S}_i = {} & (f_i - g_i \hat{g}_i^{-1}\hat{f}_i) + (1 - g_i \hat{g}_i^{-1})(-\dot{X}_{id} + \lambda_i e_i) \\ & + g_i \hat{g}_i^{-1}[-k_{1i}S_i - k_{2i}sgn(S_i)] . \end{aligned} \tag{19}$$

Consequently,

$$\begin{aligned} S_i \cdot \dot{S}_i &\le [-g_i \hat{g}_i^{-1} k_{2i} + (g_i \hat{g}_i^{-1} - 1)\hat{u}_i + \Delta f_i]|S_i| - k_{1i}S_i^2 \\ &\le [-g_i \hat{g}_i^{-1} k_{2i} + (g_i \hat{g}_i^{-1} - 1)\hat{u}_i + F_i]|S_i| \end{aligned} \tag{20}$$

If k_{2i} satisfies Equation(18), then

$$k_{2i} \ge g_i^{-1}\hat{g}_i(F_i + \eta_i) + (g_i^{-1}\hat{g}_i - 1)\hat{u}_i.$$

Therefore, we have

$$-g_i \hat{g}_i^{-1} k_{2i} + (g_i \hat{g}_i^{-1} - 1)\hat{u}_i + F_i < -\eta_i ,$$

and ultimately,

$S_i \cdot \dot{S}_i \le -\eta_i |S_i| \le 0$, which indicates the designed control

law in Equation (17) can guarantee the reachability of the sliding surface defined in Equation (15).

In order to further eliminate high frequency chattering, a continuous approximation of sgn(S) is used as

$$\mathrm{sat}(S_i/\Phi_i) = \begin{cases} \mathrm{sgn}(S_i), |S_i| \geq \Phi \\ S_i/\Phi_i, |S_i| < \Phi \end{cases}, \quad (21)$$

where $\Phi_i > 0$ is the boundary layer thickness.

Therefore, by following the above procedures of sliding mode controller design, the total forces and yaw moment used for vehicle motion control can be obtained as indicated in Equation (22).

$$F_{ud} = \begin{bmatrix} m_v(\dot{u}_d - vr - \lambda_1 e_1 - k_{11}S_1 - k_{21}\mathrm{sat}(S_1/\Phi_1)) \\ m_v(ur - \lambda_2 e_2 - k_{12}S_2 - k_{22}\mathrm{sat}(S_2/\Phi_2)) \\ I_{zz}(-\lambda_3 e_3 - k_{13}S_3 - k_{23}\mathrm{sat}(S_3/\Phi_3)) \end{bmatrix} \quad (22)$$

3.3. Servo-loop Control Design

In the servo-loop, the stabilizing forces and moment calculated from the main-loop, as shown in Equation (22), should be further distributed optimally among four tires, and furthermore, the control inputs such as longitudinal slip ratios and slip angles must be converted to actuator action.

3.3.1. Forces and moment optimal distribution mechanism

The exact conversion mechanism in this research is achieved using a sequential quadratic programming approach (Hattori *et al.*, 2002), in order to establish a dynamic trade-off between vehicle force tracking errors and control inputs within tire capability limitation.

The cost function is established firstly as follows:

$$J = \boldsymbol{E}^T \boldsymbol{W}_E \boldsymbol{E} + \Delta \boldsymbol{u}_c^T \boldsymbol{W}_{\Delta u} \Delta \boldsymbol{u}_c + \boldsymbol{u}_c^T \boldsymbol{W}_u \boldsymbol{u}_c \quad (23)$$

In the above equation, the tracking errors $\boldsymbol{E}$ are defined as the difference between desired and actual vehicle forces, i.e.

$$\boldsymbol{E} = [F_{xd} \;\; F_{yd} \;\; M_{zd}]^T - [F_x \;\; F_y \;\; M_z]^T \quad (24)$$

$\boldsymbol{u}_c$ is defined as the resultant tire longitudinal slip ratios and slip angles at each time step:

$$\boldsymbol{u}_c(k+1) = \boldsymbol{u}_c(k) + \Delta \boldsymbol{u}_c \quad (25)$$

$\Delta \boldsymbol{u}_c$ is defined as tire variables increments that need to be regulated,

$$\Delta \boldsymbol{u}_c = [\Delta s_{L1} \;\; \Delta s_{L2} \;\; \Delta s_{L3} \;\; \Delta s_{L4} \;\; \Delta \alpha_f \;\; \Delta \alpha_r]^T, \quad (26)$$

where the differences between the left and right tire slip angles are neglected.

The diagonal weighting matrices in Equation (23), i.e. $\mathbf{W_E}$, $\mathbf{W}_{\Delta \mathbf{u}}$ and $\mathbf{W_u}$, can be written as

$$\begin{cases} \mathbf{W}_E = \mathrm{diag}(\mathrm{w}_{Ex} \;\; \mathrm{w}_{Ey} \;\; \mathrm{w}_{Ez}) \\ \mathbf{W}_{\Delta u} = \mathrm{diag}(\mathrm{w}_{\Delta u1} \;\; \mathrm{w}_{\Delta u2} \;\; \mathrm{w}_{\Delta u3} \;\; \mathrm{w}_{\Delta u4} \;\; \mathrm{w}_{\Delta u5} \;\; \mathrm{w}_{\Delta u6}) \\ \mathbf{W}_u = \mathrm{diag}(\mathrm{w}_{u1} \;\; \mathrm{w}_{u2} \;\; \mathrm{w}_{u3} \;\; \mathrm{w}_{u4} \;\; \mathrm{w}_{u5} \;\; \mathrm{w}_{u6}) \end{cases} \quad (27)$$

where the elements in diag() are the diagonal elements of corresponding matrices.

The selection of weighting elements in the above equation should take both the force tracking performance and actuator limits into consideration. For example, a larger w_{Ey} value could be helpful for lateral force tracking, but considering the actuator limits, e.g. the active steering angle limits [–4deg, +4deg], the value of $\mathrm{w}_{\Delta u5}$ and $\mathrm{w}_{\Delta u6}$ should not be improperly too small.

The cost function in Equation (23) should be minimized with respect to the control input increment $\Delta \boldsymbol{u}_c$. Therefore, with appropriately selected weighting matrices $\mathbf{W_E}$, $\mathbf{W}_{\Delta \mathbf{u}}$ and $\mathbf{W_u}$, the trade-off among force tracking errors $\boldsymbol{E}$, increments of tire longitudinal slip ratios and lateral slip angles $\Delta \boldsymbol{u}_c$, and magnitudes of tire longitudinal slip ratios and lateral slip angles $\boldsymbol{u}_c$, can be achieved through Equation (28) as follows,

$$\partial J/\partial \Delta \boldsymbol{u}_c = 0. \quad (28)$$

At each time step, vehicle forces $\boldsymbol{F}_u$ can be approximated as

$$\boldsymbol{F}_u(k+1) = \boldsymbol{F}_u(k) + \boldsymbol{J}_{cob} \cdot \Delta \boldsymbol{u}_c \quad (29)$$

where $\boldsymbol{J}_{cob}$ is the corresponding Jacobian matrix, i.e.

$$\boldsymbol{J}_{cob} = \partial \boldsymbol{F}_u / \partial \boldsymbol{u}_u \quad (30)$$

Consider Equations (1) through (5) and Equation (7), the following relationship can be determined,

$$\boldsymbol{J}_{cob} = \boldsymbol{M}_F \cdot \boldsymbol{M}_{JF} \quad (31)$$

in which

$$\boldsymbol{M}_{JF}(s_{L1-4}, \alpha_f, \alpha_r) = \partial \boldsymbol{F}_t / \partial \boldsymbol{u}_c \quad (32)$$

By combining Equations (23) through (29), the desired optimal control input can be obtained as

$$\Delta \boldsymbol{u}_c^d = (\mathbf{W}_u + \mathbf{W}_{\Delta u} + \boldsymbol{J}_{cob}^T \boldsymbol{W}_E \boldsymbol{J}_{cob})^{-1} [\boldsymbol{J}_{cob}^T \boldsymbol{W}_E \cdot \tilde{\boldsymbol{E}} - \mathbf{W}_u \mathbf{u}_c(k)] \quad (33)$$

where $\tilde{\boldsymbol{E}} = \boldsymbol{F}_{ud} - \boldsymbol{F}_u(k)$, the superscript 'd' in $\Delta \boldsymbol{u}_c^d$ means 'desired', and $\boldsymbol{J}_{cob}$ can be determined through Equations (31) and (32) and the estimated longitudinal slip ratios and slip angles.

3.3.2. Actuator control

The optimal control inputs given by Equation (33), i.e. the increments of tire slip angle and longitudinal slip ratio, should be further converted to the actuator (tire/wheel) control inputs, i.e. active steering angles for tire slip angle control and actual wheel torques T_c for wheel slip ratio control.

By neglecting steering system dynamics, the desired steering angle increments $\Delta \delta_i^d$ are considered identical as the desired slip angle increments $\Delta \alpha_i^d$, i.e.

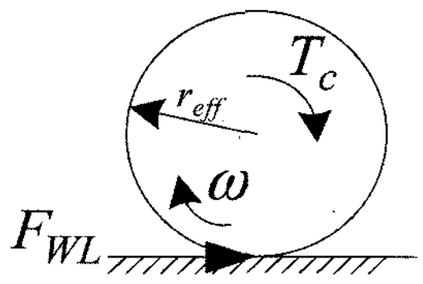

Figure 5. Wheel model.

$$[\Delta\delta_f^d \;\; \Delta\delta_r^d] \approx [\Delta\alpha_f^d \;\; \Delta\alpha_r^d]^T. \tag{34}$$

As for slip ratio control, referring to Figure 5, the following first order wheel dynamics is considered

$$J_W\dot{\omega} = -F_{WL} \cdot r_{eff} + T_c, \tag{35}$$

where the control torque T_c for the front wheel is always constrained to be a braking torque; and for rear wheels (driven wheels), T_c also depends on whether an accelerating or braking action is required. A nonlinear PI controller is used for the actual slip ratio regulation (Van Zanten *et al.*, 1996), i.e.

$$T_c = F_{WL} \cdot \mathrm{r}_{eff} + \mathrm{K}_p(\mathrm{s}_L^d - \mathrm{s}_L) + (\mathrm{s}_L^d - \mathrm{s}_L)K_i/s, \tag{36}$$

where **s** is the Laplace operator, F_{WL} is tire wheel plane longitudinal force as shown in Figure 5, $\mathrm{K_p}$ and $\mathrm{K_i}$ are proportional and integral gains as control parameters, s_L^{d} and s_L are the desired and actual longitudinal slip ratios, respectively. Combining Equation (25), (26) and (33), s_L^{d} can be obtained as

$$\mathrm{s}_L^d = s_L(k) + \Delta s_L^d \tag{37}$$

4. SIMULATIONS AND ANALYSIS

The presented control integration based on main/servo-loop structure is evaluated through several computer simulations, which are carried out on a nonlinear vehicle model with nonlinear tires including transient properties. The model contains ten DOFs: six DOFs for the rigid vehicle body, i.e. longitudinal, lateral, vertical, yaw, pitch and roll motions; four other DOFs for wheel rotation. In particular, load transfer due to longitudinal and lateral acceleration is also taken into account.

For comparison among different chassis control systems with the same control structure, namely 'main/servo-loop', simulations are carried out for three vehicles with different configurations, i.e. the vehicle equipped with longitudinal slip ratio control (LSC) only, four wheel steering (4WS) only, and the integrated (INT) control vehicle equipped with their combination. Since control integration (INT) can take advantage of both subsystems through coordination, two different INT controllers with different weighting matrices of control inputs for force distribution are designed, while INT1 has the combined weighting matrices of 4WS and LSC subsystems, and INT2 has the redesigned weighting matrices that can bring further potential benefits of integrated control.

4.1. Sinusoidal Steer Maneuver

With an initial speed of 120 km/h (33 m/s), a 5 deg sinusoidual front steering angle is applied to the vehicle with 2 sec period. The vehicle responses and comparison results are shown in Figure 6. Apparently as shown in Figure 6a, LSC can follow neither the desired yaw rate nor vehicle sideslip angle well, which confirms that the limitations of LSC to provide sufficient lateral forces, especially with large tire slip angles. On the other hand, vehicles equipped with 4WS and INT configurations, particularly INT2 case, can follow the desired yaw rate quite well and regulate the sideslip angle within a relatively acceptable value of 0.7 deg. This indicates the evident improvement in handling and stability performances can be achieved by control integration based on force and moment optimum distribution among wheels.

The control effect can also be reflected through dynamic tire workload, which is defined as the ratio of the horizontal force over the normal force for each tire, i.e.

$$\eta_{WKLD\_i} = \sqrt{\frac{F_{Li}^2 + F_{Si}^2}{F_{Zi}^2}} \tag{38}$$

As indicated in Figure 6b, vehicles with 4WS and INT controllers show lower tire workload than that of LSC case, i.e. INT and 4WS still preserve a large lateral stability margin while the tire force utilization of LSC case has already reached saturation region of tire/road adhesion. Although the tire workload of 4WS is slightly lower than that of INT cases, in considering the better tracking performances of yaw rate and vehicle sideslip of INT controllers, the higher tire workload of INT cases means that the integrated controllers can use the tire friction forces more effectively.

Figure 6c and 6d shows the different control input demands for various configurations. Compared with LSC configuration, wheel torque demands for longitudinal slip ratio control in INT case are reduced significantly, while the active steering demands for INT and 4WS cases are all within the limited steering angle range of [−4 deg, 4 deg].

4.2. Step Steer Maneuver

A step steer maneuver simulation with an equivalent front steering angle of 6 deg is performed for the vehicle driving on dry asphalt road with an initial forward speed of 120 km/h (33 m/s).

As can be seen in Figure 7a, the yaw rate and vehicle sideslip in LSC case are far from their desired values, which indicates that the vehicle will spin around z-axis

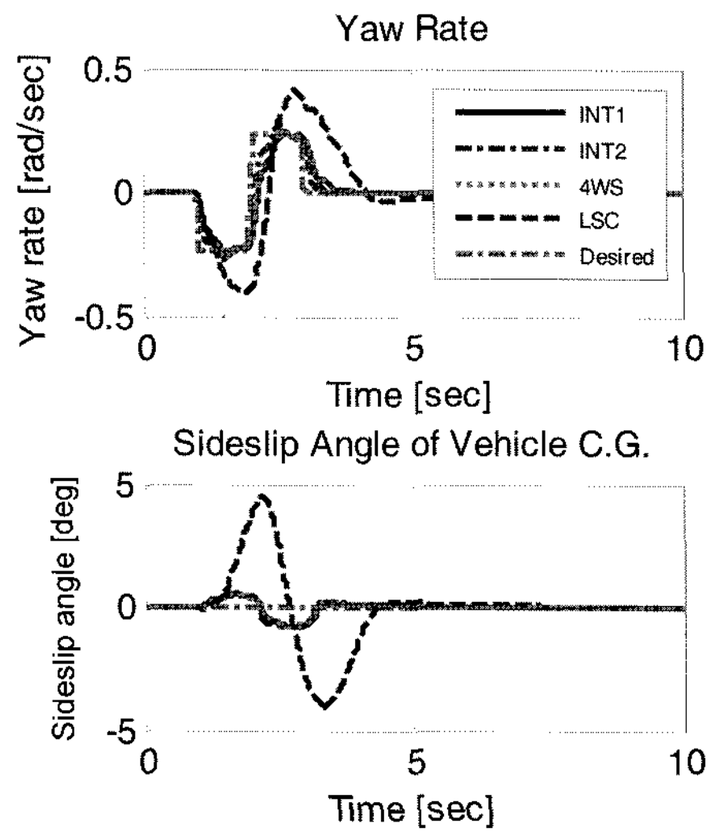

(a)

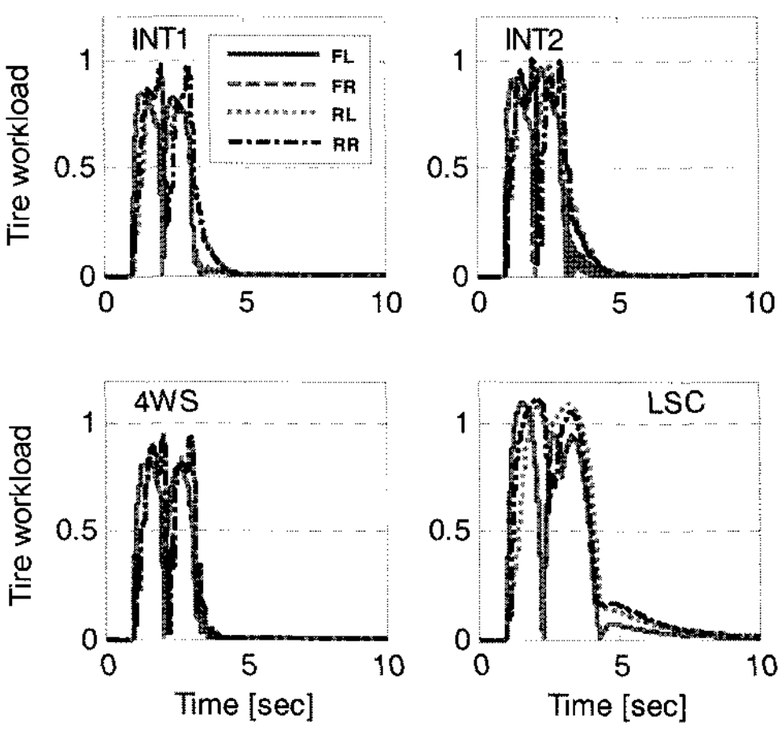

(b)

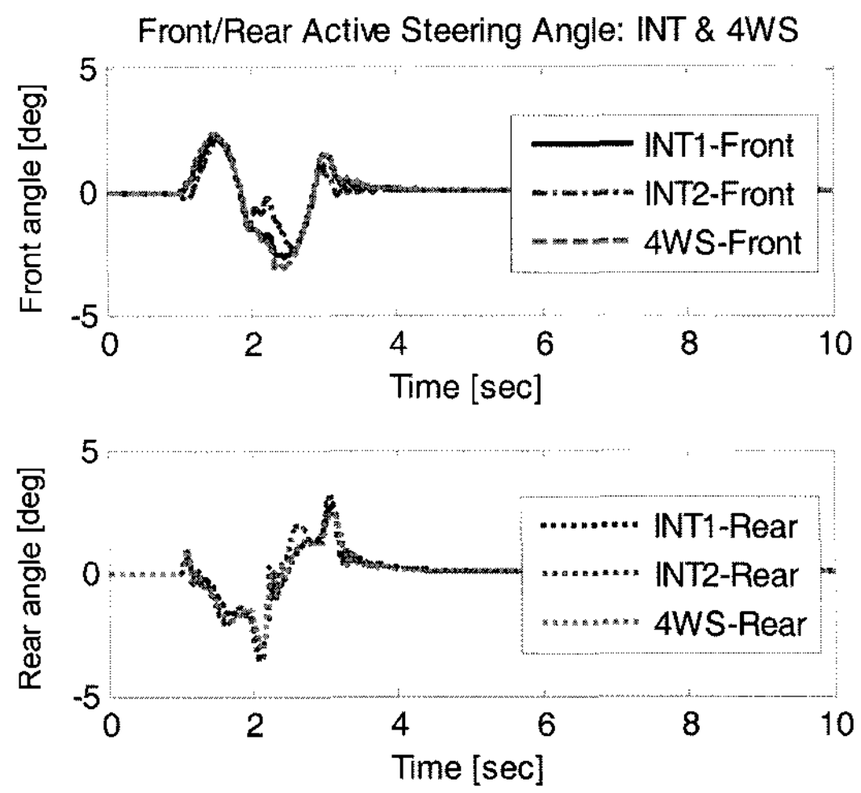

(c)

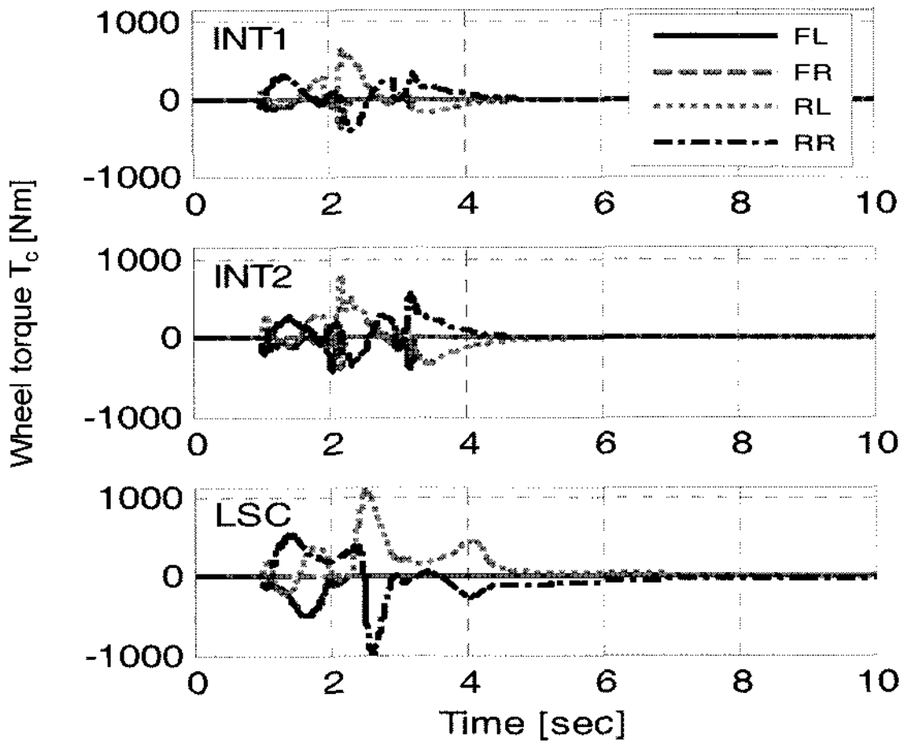

(d)

Figure 6. Sinusoidal steer maneuver.

drastically. This again confirms that LSC becomes less effective when a much larger lateral force and a larger yaw moment are needed, for that LSC can only generate a limited stabilizing yaw moment through differential longitudinal forces between left and right tires.

On the other hand, 4WS and INT can track the desired yaw rate and vehicle sideslip quite well; however, compared to the vehicle with 4WS only, the vehicles with INT1 and INT2, especially INT2, respond to the steer input more quickly and furthermore, less overshoot in yaw rate response is presented. This again confirms the considerable improvement by control integration of 4WS and LSC subsystems.

As for tire workload comparisons in Figure 7b, INT2 controller shows the lowest workload in addition to its best performance of yaw rate and sideslip tracking, which means that by the coordination between subsystems, INT2 can utilize the tire/road adhesion capability effectively to a larger extent.

Furthermore, Figure 7c shows the front and rear active steering angles of INT and 4WS vehicles. Due to the extremely large value of desired stabilizing yaw moment, which is needed to correct the yaw motion, the front and rear axles in both cases are steered in reversed direction. Since INT can use both differential longitudinal forces and active steering to obtain a corrective yaw moment, the active steering angle demand of INT2 is slightly more favorable than that in 4WS case.

4.3. Braking under μ-split Condition

In this simulation, the vehicles equipped with the above three control systems, i.e. INT, 4WS and LSC, are braking on μ-split road with adhesion coefficients of $\mu_{H\_left} = 1.2$ and $\mu_{L\_right} = 0.2$. The initial speed is 14 m/s and

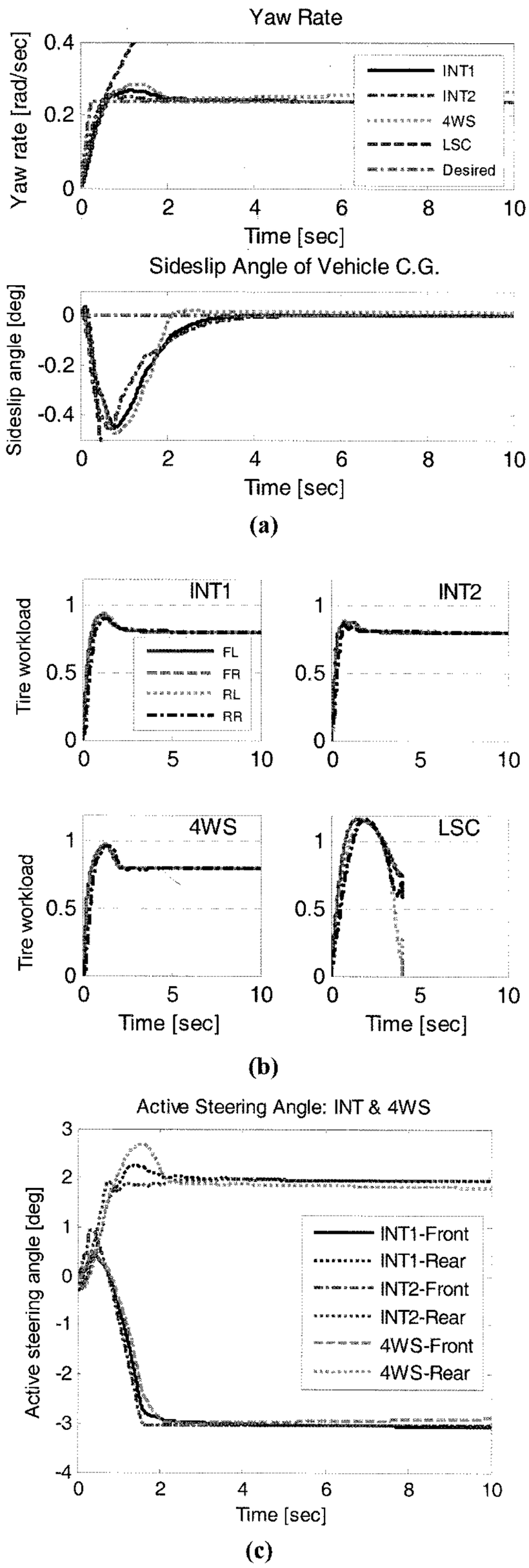

Figure 7. Step steer maneuver.

the deceleration is –0.3 g. Figure 8 shows the simulation results of vehicle responses and control inputs.

As can be seen in Figure 8a, although the driver steering command is zero, the destabilizing yaw moment due to uneven tire/road adhesion condition has the greatest effect on the vehicle with LSC, which results in an unfavorable lateral deviation larger than 3 meters, and thus the straight running ability of the vehicle is considerably impaired. However, both INT and 4WS cases exhibit acceptable performances of path following and stability, while compared with 4WS, INT could still provide enough braking force and thus track the longitudinal velocity quite well, so the stopping time and distance are much less, as shown in Figure 8b.

This is because, in LSC and 4WS cases, the adhesion capability of tires with high-μ, i.e. the left side, can not be effectively utilized as in INT case, considering the tire workload as shown in Figure 8c. Particularly, in LSC case, the tire workload of the real left tire is only around 0.4, while it is much worse that the tire workloads of all four tires in 4WS case are less than 0.4.

Furthermore, as shown in Figure 8d, due to control coordination, the applied control torque in INT case for the rear left wheel is larger than that in LSC. Therefore, differently from LSC case, this tire utilizes the adhesion more effectively, with a tire workload around 0.5.

Based on the above results and analysis, a unique and overwhelming merit of presented chassis control integration is clear from Figure 6 through 8, that is, compared with stand-alone control systems, significant performance improvement can be achieved by control coordination.

5. CONCLUSIONS

In this paper, by using sliding mode control in the main-loop and nonlinear optimizing algorithm for force distribution in the servo-loop, the integrated chassis control, which coordinates the control actions of stand-alone 4WS and LSC, has been investigated. It is based on the fact that both 4WS and LSC can influence the lateral dynamics but 4WS can be effective only in low to mid-range lateral acceleration, while LSC can help to produce a corrective yaw moment even under critical driving conditions. Theoretical analysis and computer simulation studies further clarify the following points:

(1) With the proposed main/servo-loop structure, tire nonlinearities are moved to the servo-loop of the controller. In other words, the tire is treated as a special kind of actuator, which makes the main-loop controller design easier and more effective, e.g. sliding mode controller in our case.

(2) Based on sequential quadratic programming approach, the optimal distribution of forces and moment among four tires can be achieved. Although the optimal distribution is not updated real time, as soon as the time step is small enough, the optimization process carried out in every time step can make sure that the

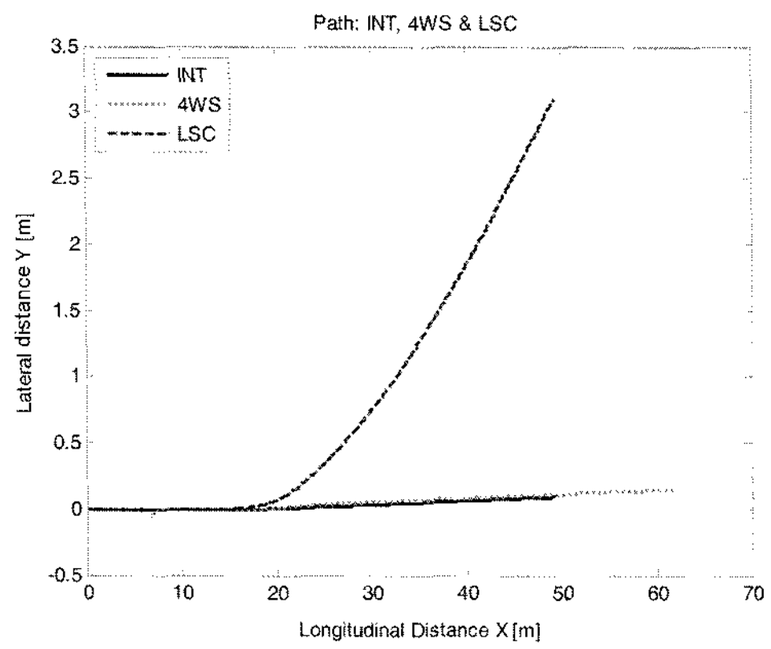

(a)

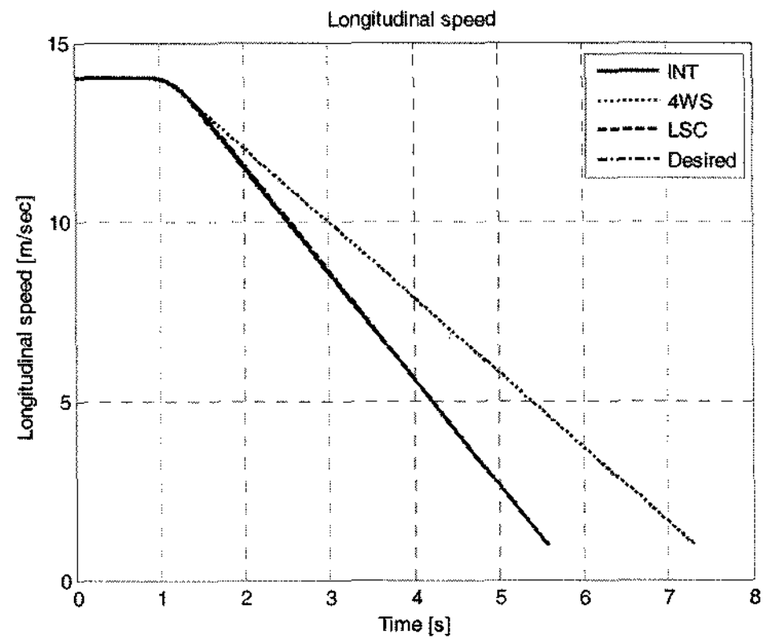

(b)

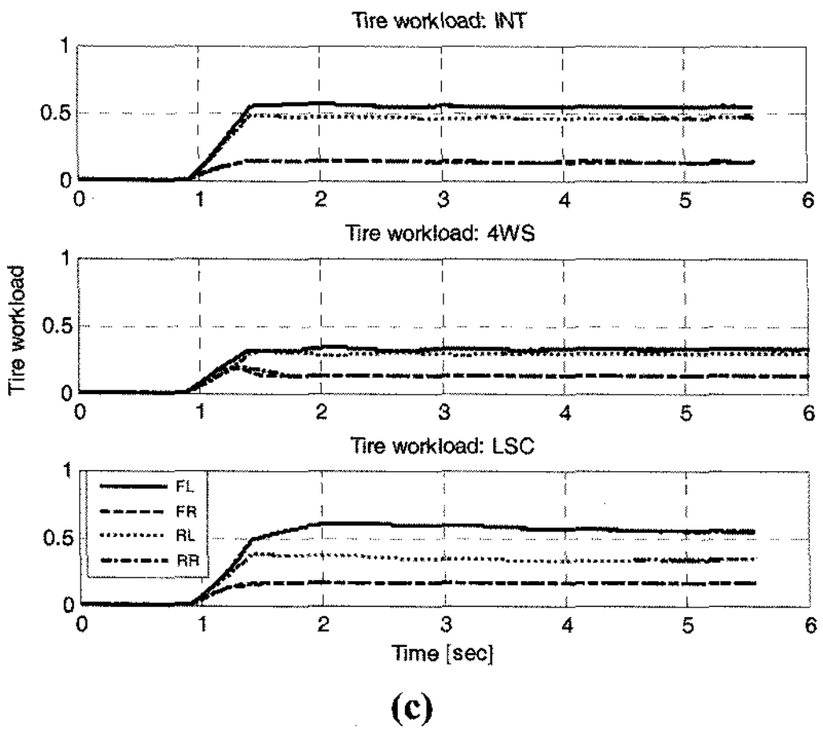

(c)

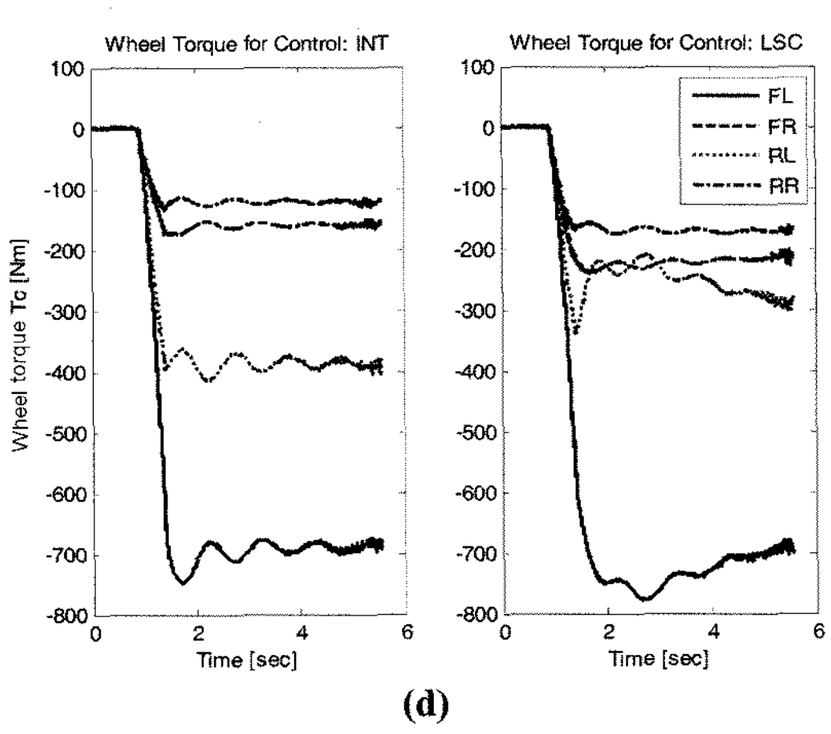

(d)

Figure 8. Braking on μ-split road maneuver.

forces and moment are distributed in such a way that the tire/road adhesion can be utilized more effectively, especially under low-μ conditions.

(3) Owing to the excellent tracking performances of both sliding mode controller and nonlinear optimizing method for force and moment distribution, the desired yaw and sideslip motions of vehicle can be well tracked by the proposed chassis control integration, compared with stand-alone LSC or 4WS controllers. Furthermore, since the proposed integration is not a simple combina-tion of the two subsystems, the control coordination between them could bring additional benefits of a maximized handling performance and stability margin.

(4) In this control scheme, values of vehicle states, including many states difficult to measure, are required. Therefore, in order to save the sensor cost, accurate and effective estimators should be designed in the future work.

ACKNOWLEDGEMENT–The authors are grateful for the financial support provided by National Natural Science Foundation of China. Additionally, we would like to thank the anonymous reviewers who gave us many valuable advices and suggestions for improvements of this paper.

REFERENCES

Cherouat, H., Lakehal-Ayat, M. and Diop, S. (2004). An integrated braking and steering control for a cornering vehicle. *Proc. AVEC'04.* 341–346.

Fruechte, R. D., Karmel, A. M., Rillings, J. H., Schilke, N. A., Boustany, N. M. and Repa, B. S. (1989). Integrated vehicle control. *IEEE 39th Vehicular Technology Conf.*, **2,** 868–877.

Furukawa, Y. and Abe, M. (1997). Advanced chassis control systems for vehicle handling and active safety. *Vehicle System Dynamics*, **28**, 59–86.

Harada, M., and Harada, H. (1999). Analysis of lateral stability with integrated control of suspension and steering systems. *JSAE Review* **20, 4**, 465–470.

Hattori, Y., Koibuchi, K. and Yokoyama, T. (2002). Force and moment control with nonlinear optimum distribution for vehicle dynamics. *Proc. AVEC'02,* 595–600.

Horiuchi, S., Okada, K. and Nohtomi, S. (1999). Improvement of vehicle handling by nonlinear integrated control of four wheel steering and four wheel torque. *JSAE Review*, **20**, 459–464.

Kawakami, H., Sato, H., Tabata, M., Inoue, H. and Itimaru, H. (1992). Development of integrated system between active control suspension. Active 4WS, TRC and ABS, *SAE Paper No.* 920271, 326–333.

Kiencke, U. and Nielsen, L. (2000). *Automotive Control Systems.* SAE Inc.. Springer-Verlag Berlin Heidelberg.

Kim, S. J., Kwak, B. H., Chung, S. J. and Kim, J. G. (2006). Development of an active front steering system. *Int. J. Automotive Technology,* **7, 3,** 315–320.

Manning, W., Crolla, D., Brown, M. and Selby, M. (2000). Co-ordination of chassis subsystems for vehicle motion control. *Proc. AVEC'2000,* 313–319.

Mokhiamar, O. and Abe, M. (2004). Simultaneous optimal distribution of lateral and longitudinal tire forces for the model following control. *J. Dynamic Systems, Measurement, and Control*, **126**, 753–763.

Nouillant, C., Assadian, F., Moreau, X., and Oustaloup, A. (2002). A cooperative control for car suspension and brake system. *Int. J. Automotive Technology* **3, 4**, 147–155.

Shen, X., Li, D. and Yu, F. (2006). Study on vehicle chassis control integration based on general actuator-plant structure. *Proc. AVEC'2006.* (accepted)

Shino, M., Raksincharoensak, P. and Nagai, M. (2002). Vehicle handling and stability control by integrated control of direct yaw moment and active steering. *Proc. AVEC'2002.* 25–31.

Slotine, E. and Li, W. (1991). *Applied Nonlinear Control.* Prentice-Hall. New Jersey.

Smakman, H. (2000). Functional integration of active suspension with slip control for improved lateral vehicle dynamics. *Proc. AVEC'2000.* 397–404.

Valasek, M., Vaculin, O., and Kejval, J. (2004). Global chassis control: Integration synergy of brake and suspension control for active safety. *Proc. AVEC'2004.* 495–500.

Van Zanten, A., Erhardt, R., Pfaff, G., Kost, F., Hartmann, U. and Ehret, T. (1996). Control aspects of the bosch-VDC. *Proc. AVEC'96,* 573–608.

Yokoya, Y., Kizu, R., Kawaguchi, H., Ohashi, K. and Ohno, H. (1990). Integrated control system between active control suspension and four wheel steering for the 1989 CELICA. *SAE Paper No.* 901748, 1546–1561.